Investigation of local symmetry effects on the electronic structure of manganites: Hexagonal $YMnO_3$ versus orthorhombic $LaMnO_3$

Deok-Yong Cho,[1,*] S.-J. Oh,[1] Dong Geun Kim,[1] A. Tanaka,[2] and J.-H. Park[3,†]
[1]*Department of Physics and Astronomy, Seoul National University, Seoul 151-747, Korea*
[2]*Department of Quantum Matter, ADSM, Hiroshima University, Higashi-Hiroshima 739-8526, Japan*
[3]*Department of Physics and eSSC, Pohang University of Science and Technology, Pohang 790-784, Korea*
(Received 16 October 2008; revised manuscript received 9 December 2008; published 21 January 2009; corrected 26 January 2009)

The local site symmetry effects on electronic structure of manganites were investigated by using theoretical analyses in terms of the cluster model calculations for the O *K*- and Mn $L_{2,3}$-edge x-ray-absorption spectroscopy (XAS) results of hexagonal $YMnO_3$ and orthorhombic $LaMnO_3$. $YMnO_3$, which has an unusual MnO_5 (D_{3h}) site symmetry, exhibits remarkably different electronic structure and XAS line shape from those of $LaMnO_3$ with the conventional MnO_6 (D_{4h}) site symmetry, despite the same Mn^{3+} ($3d^4$) trivalent ionic state. We developed an algebraic formalism, which takes into account the crystal-field energies and hybridization strengths of the D_{3h} Mn $3d$ orbital in $YMnO_3$. The deduced values are very consistent with the first-principles local-density approximation plus Hubbard U calculation results. The cluster model calculations involving the different site symmetries well reproduce the O *K*-edge and Mn $L_{2,3}$-edge spectra of both manganites. In the analyses of the O *K*-edge spectra, we also took into account the Y $4d$ and La $4f/5d$ orbital states.

DOI: 10.1103/PhysRevB.79.035116 PACS number(s): 78.70.Dm, 71.70.Ch

I. INTRODUCTION

Hexagonal manganites ($RMnO_3$, where R=Ho-Lu or Y, Sc, and In) have attracted much attention due to their interesting multiferroicity and unusual magnetoelectric coupling behaviors.[1–7] Below $T_C \sim 900$ K, large ferroelectric (FE) displacements occur at R ion sites along the hexagonal c axis with collective rotations of rigid MnO_5 cages.[8] Below $T_N \sim 100$ K, the antiferromagnetic (AFM) spin order is developed with geometrical frustration in the basal Mn^{3+} sublattices.[9]

The MnO_5 bipyramidal local structure, which results in peculiar local electronic states, has been discussed in relation with the unusual coupling behaviors[3–5] and also evoked diverse arguments for the origin of the ferroelectricity such as a "directional d^0-ness" and electrostatic dipole interactions.[8,10] Recently, in the x-ray-absorption spectroscopy (XAS) study, we have demonstrated that not only MnO_5 but also RO_8 local structures play essential roles in the multiferroicity of the hexagonal manganites.[11] Further, neutron-scattering studies on $YMnO_3$ showed that the magnetoelectric intercoupling can be attributed to strong Mn-O-Y bond chains.[12] Hence, it is important to understand in detail the electronic states of MnO_5 and RO_8 local structures and their interactions in hexagonal $RMnO_3$. The electronic states strongly depend not only on the electron-electron correlations but also on the crystal field (CF) and the metal d-oxygen $2p$ hybridizations, which are determined by the site symmetries and the characteristic local environments.[13]

The degenerated atomic levels split in the solid due to the site symmetry lowering resulting in the CF. The CF, which results from the interionic Coulomb energies, determines the crystal orbital state energies in corporation with their hybridizations with the electron states in the nearest-neighbor ions. The XAS provides direct information on the local electronic states and their intermixing with neighboring ions. The O *K*-edge XAS, $1s \rightarrow 2p$, exhibits the unoccupied O $2p$ states, which are strongly hybridized with Mn $3d/4sp$ and Y $4d/5sp$ states, and represents the unoccupied Mn $3d/4sp$ and Y $4d/5sp$ electronic states in the prototype hexagonal manganite $YMnO_3$. Further the more detailed information on the Mn $3d$ electronic states can be obtained from the Mn $L_{2,3}$-edge XAS, which utilizes the Mn $2p \rightarrow 3d$ dipole transition.

The energy-level splitting in the hexagonal crystal with D_{3h} (MnO_5) and D_{3d} (YO_8) site symmetries can be simply derived from the interionic Coulomb energies in the group theoretical approach, and this scheme has already been adopted for explaining the overall Mn d-d level splits in the optical measurements such as the second-harmonic generation experiment.[14] Since the energy range of the level splitting is much smaller than the O $2p \rightarrow$ Mn $3d$ charge-transfer energy ($\gtrsim 4$ eV), the interaction between Mn $3d$ and O $2p$ orbitals was generally neglected in the optical investigation. However, the simple d-d split in the symmetry argument is not sufficient to understand the interactions between Mn/Y d and O $2p$ orbitals. Further, the electronic structure in the wide energy range obtained by the x-ray techniques such as photoemission, photoabsorption, and scattering should be understood based on the many-body approach often utilizing either the Anderson impurity Hamiltonian or the cluster model calculations with the configuration interactions (CIs). In this approach, the CF and the d-p hybridization effects should be taken into account more explicitly. Therefore in this paper, we derive the formulas for the CF and the metal d-oxygen $2p$ hybridization separately and analyze the O *K*- and Mn $L_{2,3}$-edge XAS spectra in terms of the cluster model calculation with CIs including full atomic multiplets.

As seen in the XAS results,[11] the spectral line shape barely changes with the choice of R in the hexagonal $RMnO_3$, indicating that the electronic structure is mostly determined by the site symmetry. Thus it is worthy to determine the CF energies and the hybridization strengths through a simple algebraic method instead of the full band calcula-

tions based on the local-density approximation (LDA) or LDA+Hubbard U. This simple approach is intuitive and generally applicable to all the hexagonal systems with the same site symmetry. Further, it can be also integrated with many-body model calculations such as the cluster model calculations, which are established to well describe the electronic structure of the 3*d* transition-metal oxides.

We focus on constructing the generalized calculation schemes for the CF and the metal *d*-oxygen 2*p* hybridization strengths in the hexagonal $R\mathrm{MnO_3}$. To verify the validity of the methodologies, we also applied the same procedure onto the well-known orthorhombic crystal structure and this turned out to successfully describe the local electronic structure of the orthorhombic crystal such as $\mathrm{LaMnO_3}$. The pedagogic descriptions in this paper will enable the reader to easily understand the gigantic difference in the electronic structure of hexagonal $R\mathrm{MnO_3}$ from orthorhombic manganites as the simple influence of the local symmetry. The rest of paper is summarized as follows. In Sec. II, we present generalized approaches to the CF energies and hybridization strengths for the Mn *d* and Y *d* states in the hexagonal $\mathrm{YMnO_3}$. In Sec. III, we present the cluster model calculation analysis results, which successfully reproduce the O *K*- and Mn $L_{2,3}$-edge XAS spectra of the hexagonal $\mathrm{YMnO_3}$ with $\mathrm{MnO_5}$ (D_{3h}) and the orthorhombic $\mathrm{LaMnO_3}$ with $\mathrm{MnO_6}$ (D_{4h}) at the same trivalent ionic state $\mathrm{Mn^{3+}}$ ($3d^4$). The consistency with the results of an LDA+U calculation is discussed in Sec. IV. Section V gives the summary and conclusions of this work and the orbital hybridizations in the $\mathrm{MnO_5}$ bipyramid and $\mathrm{MnO_6}$ octahedron are compared in an alternative method in the Appendix.

II. LOCAL INTERACTIONS IN $\mathrm{YMnO_3}$

In insulating oxides such as $R\mathrm{MnO_3}$, the overall electronic structure can be described by the local nearest-neighbor interactions although the details are modified by the interactions with other neighbors. Here we present theoretical electronic structure calculated within a single cluster (MO_n; $M=R$ and Mn) model, which takes into account the nearest-neighbor interactions. In hexagonal $\mathrm{YMnO_3}$, the Mn ion is surrounded by three planar and two apical oxygen ions ($\mathrm{MnO_5}=\mathrm{MnO_P^3O_T^2}$), which form a bipyramid cage, while the Y ion is surrounded by eight oxygen ions ($\mathrm{YO_8}=\mathrm{YO_T^6O_P^2}$). Note that the conventionally denoted O_P (in-plane oxygen) and O_T (on-top oxygen) in $\mathrm{YMnO_3}$ (Ref. 8) correspond to planar and apical oxygen ions in the $\mathrm{MnO_5}$ cage while they become opposite in the $\mathrm{YO_8}$ cage. The actual shapes of the two cages in the crystal structure are shown in Fig. 1. There are crystallographically one Mn site, four different oxygen sites, and two different yttrium sites, which are conventionally denoted as Mn, $\mathrm{O^1}$-$\mathrm{O^4}$, and $\mathrm{Y^1}/\mathrm{Y^2}$, respectively.[15]

The details of $\mathrm{MnO_5}$ and $\mathrm{YO_8}$ local structures are shown in Fig. 1(b). In a $\mathrm{MnO_5}$ bipyramid with a D_{3h} site symmetry, the Mn-O bonds consist of three and two nearly identical planar and apical bonds, respectively, even under the ferroelectric distortions ($P6_3cm$). The ratio of the apical to planar bond length, $d(\mathrm{Mn\text{-}O_T})/d(\mathrm{Mn\text{-}O_P})$, is approximately 0.9. The situation is somewhat complicated in the $\mathrm{YO_8}$ cage.

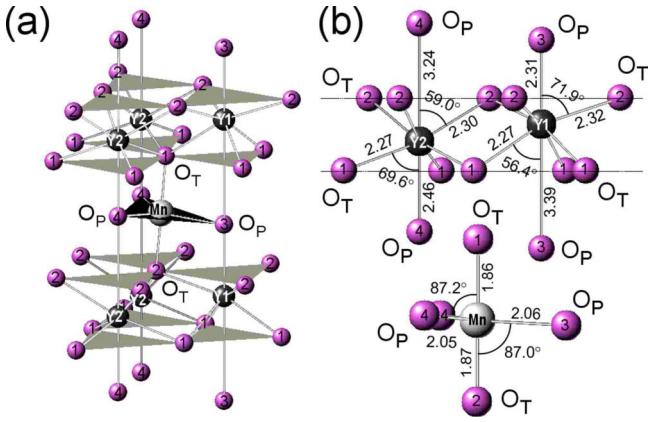

FIG. 1. (Color online) (a) Crystal structure and (b) $\mathrm{YO_8}$ and $\mathrm{MnO_5}$ local structures of $\mathrm{YMnO_3}$ at room temperature. The atomic positions were taken from Ref. 12. Two yttrium sites are denoted by $\mathrm{Y^1}$ and $\mathrm{Y^2}$ and the sites of on-top (O_T) and in-plane (O_P) oxygen ions are denoted by 1,2 and 3,4, respectively. The oxygen triangles which are the units of calculations for Y/Mn-O hybridization strengths are explicitly shown.

There are two different yttrium sites, one with upward displacement ($\mathrm{Y^1}$) and the other with downward displacement ($\mathrm{Y^2}$). The site ratio of $\mathrm{Y^1}:\mathrm{Y^2}$ is 1:2. As can be seen in the figure, the Y-O bond lengths vary for different oxygen ions ($\mathrm{O^1}$-$\mathrm{O^4}$), but both $\mathrm{O^1}$ and $\mathrm{O^2}$ always keep the threefold symmetry around the $\mathrm{O^3(O^4)}$-$\mathrm{Y^1(Y^2)}$-$\mathrm{O^3(O^4)}$ line. Then the site symmetry becomes a quasitrigonal and the CF and hybridization strengths are calculated numerically under the trigonal symmetry (D_{3d}). The energy-level splittings for various relevant metal oxygen coordination and site symmetries, MO_5 (D_{3h}), MO_6 (O_h, D_{4h}, and D_{3d}), and MO_8 (D_{3d}) are schematically illustrated in Fig. 2.[16] It is noticeable that both $\mathrm{MnO_5}$ and $\mathrm{YO_8}$ cages consist of apical bonds and planar bonds forming triangles. Thus one can simplify the calculations for CF and hybridization strengths by taking advantage of the triangular base symmetry, which are described in Secs. II A and II B.

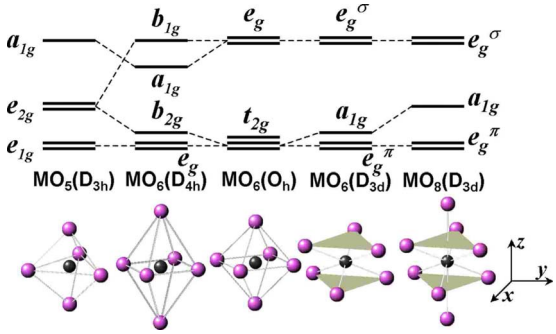

FIG. 2. (Color online) Energy splittings and orbital symmetries for various MO_n (M: Y or Mn) local structures. The *d* orbital in the $\mathrm{MnO_5}$ is split into e_{1g} (yz/zx), e_{2g} [$(x^2-y^2)/xy$], and a_{1g} ($3z^2-r^2$) orbitals under the bipyramidal D_{3h} symmetry. $\mathrm{YO_8}$ has a quasitrigonal D_{3d} symmetry and the *d* orbital is split into a_{1g} ($3z^2-r^2$) and e_g^π/e_g^σ [mixtures of yz/zx and $(x^2-y^2)/xy$]. The *d* orbital in $\mathrm{MnO_6}$ under the D_{4h} symmetry with a long *z* axis as in orthorhombic $\mathrm{LaMnO_3}$ is split into e_g (yz/zx), b_{2g} (xy), a_{1g} ($3z^2-r^2$), and b_{1g} (x^2-y^2).

A. Crystal fields

In an MO_n cluster, CF energies of the electron at the central ion are often presented by the expectation values of the electrostatic potential energy contributed by point charges at the positions of oxygen ions with effective charge number $-Z$. Within the first-order perturbation, the one-electron CF energies are given by

$$U^{\mathrm{CF}}_{mm'} = Z\sum_{i=1}^{n}\left\langle m\left|\frac{1}{|\vec{r}-\vec{a}_i|}\right|m'\right\rangle, \tag{1}$$

where $\vec{a}_i$ stands for the n oxygen positions from the central one and m,m' are magnetic quantum numbers of the electron orbital states. In the case of d orbital, these can be rewritten as

$$U^{\mathrm{CF}}_{mm'} = Z\sum_{k=0,2,4;m''=-4,-3,\ldots,+3,+4} A_{km''}\langle r^k\rangle c^k(2m,2m')\delta_{m'',m-m'}, \tag{2}$$

where r is in unit of the bond length and $c^k(lm,l'm')$ and $A_{km''}$ are Gaunt coefficients[17] and structural coefficients,[16] respectively.

1. D_{3h} crystal field in MnO_5 bipyramid

In the MnO_5 cluster, the matrix representation for the one-electron CF energies can be simplified by introducing a contraction factor $\kappa = d(\text{Mn-O}_T)/d(\text{Mn-O}_P)$. The CF energy matrix has a diagonal form even in the basis of unperturbed d orbitals as follows:

$$\{U^{\mathrm{CF}}_{mm'}\} = \begin{pmatrix} \alpha & 0 & 0 & 0 & 0 \\ 0 & \beta & 0 & 0 & 0 \\ 0 & 0 & \gamma & 0 & 0 \\ 0 & 0 & 0 & \beta & 0 \\ 0 & 0 & 0 & 0 & \alpha \end{pmatrix} \quad \text{for Mn } 3d,$$

$$\alpha \equiv -\frac{2}{7}A_{20}\langle r^2\rangle + \frac{1}{21}A_{40}\langle r^4\rangle,$$

$$\beta \equiv +\frac{1}{7}A_{20}\langle r^2\rangle - \frac{4}{21}A_{40}\langle r^4\rangle,$$

$$\gamma \equiv +\frac{2}{7}A_{20}\langle r^2\rangle + \frac{6}{21}A_{40}\langle r^4\rangle, \tag{3}$$

for $m,m' = (+2,+1,0,-1,-2)$, and the coefficients are found to be $A_{20} = Z(4-3\kappa)/2\kappa^3$ and $A_{40} = Z(16+9\kappa)/8\kappa^5$, respectively, for r in unit of the Mn-O_T bond length.

Since the one-electron energy matrix is already diagonal in the bipyramidal field, the degeneracies of both $|\pm 1\rangle$ and $|\pm 2\rangle$ are maintained. Thus one can choose the real-space basis of $d_{3z^2-r^2}(m=0)$, $d_{yz,zx}(m=\pm 1)$, and $d_{x^2-y^2,xy}(m=\pm 2)$. The degeneracies are independent of the Mn-O_T bond length along the z direction, i.e., the ratio κ.

It should be noted that, in the O_h field,[18] A_{20} vanishes and the CF splitting energy 10 Dq is determined solely by the $\langle r^4\rangle$ terms, while in this D_{3h} field, A_{20} survives and further the first $\langle r^2\rangle$ term is comparable to the second $\langle r^4\rangle$ term. The CF energies are determined by the ratios of these two terms, which vary with the contraction factor κ. The energy of the singlet a_{1g} $(3z^2-r^2)$ turns out to be always highest while the energy of yz/zx is either higher or lower than that of $(x^2-y^2)/xy$ depending on κ (e_{1g},e_{2g} denote conventionally these two doublets according to the energy order). In $YMnO_3$ with $\kappa \simeq 0.9$, the CF splitting energy $(\gamma-\alpha)$, the energy difference between a_{1g} and e_{2g}, is estimated to be approximately equal to $(\alpha-\beta)$, the energy difference between e_{2g} and e_{1g} for $\langle r^4\rangle/\langle r^2\rangle = 2-4$.[19]

2. D_{3d} crystal field of YO_8

The CF of YO_8 cage onto Y $4d^0$ can be calculated in a similar fashion. The CF energy matrix is found to have forms

$$\{U^{\mathrm{CF}}_{mm'}\} = \begin{pmatrix} \alpha & 0 & 0 & -\delta & 0 \\ 0 & \beta & 0 & 0 & \delta \\ 0 & 0 & \gamma & 0 & 0 \\ -\delta & 0 & 0 & \beta & 0 \\ 0 & \delta & 0 & 0 & \alpha \end{pmatrix} \quad \text{for Y } 4d,$$

where α, β, and γ are given as in Eq. (3) and

$$\delta \equiv \frac{\sqrt{35}}{21}A_{43}\langle r^4\rangle \tag{4}$$

as long as the crystal has the $P6_3cm$ symmetry with the threefold symmetry for both O^1 and O^2 triangles (see Fig. 1). Differently from the Mn $3d$ matrix, Y $4d$ matrix has nonvanishing off-diagonal elements $(\mp\delta)$ which intermix $m=\pm 2$ and $m=\mp 1$ states (signs in same order). The δ term is much larger than all the other terms, so that the highly mixed $|\pm 2\rangle \oplus |\mp 1\rangle$ form degenerated bonding (e_g^{π}) and antibonding (e_g^{σ}) states with a large energy separation and the energy level of the unmixed $|0\rangle$ singlet (a_{1g}) stays nearly at the middle (see Fig. 2). In $YMnO_3$, the a_{1g} level lies slightly above (60% for Y^1) and below (40% for Y^2) the middle (50%) of the e_g^{π} and e_g^{σ} energy levels for $\langle r^4\rangle/\langle r^2\rangle = 2-4$.[19]

B. Hybridization strengths

The central Mn $3d$ and Y $4d$ orbitals overlap only with the oxygen $2p$ electron clouds with the same orbital symmetries. Thus the hybridization matrix has the same form of the matrix as the CF energy matrix presented in Sec. II A except for replacements of $A_{km''}\langle r^k\rangle$ with hybridization coefficients $\tilde{V}_{km''}$. The hybridization coefficients were estimated by using bond-orbital model of Harrison[20] and the differences in the interatomic distances were taken into account. According to the Harrison rule, the hybridization coefficients are proportional to $a^{-3.5}$ (a: the interatomic distance) for p-d hybridization.[20] The coefficients $\tilde{V}_{km''}$ can be transformed into $V_{mm'}$ in the same fashion for the CF energies $U^{\mathrm{CF}}_{mm'}$ in Sec. II A.

1. Hybridization strengths in a MnO_5 bipyramid

For MnO_5 bipyramid, the hybridization comes from two apical bonds (Mn $3d$-O_T $2p$) and three planar ones

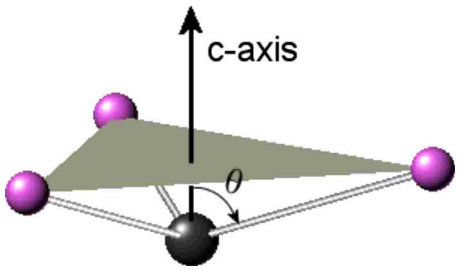

FIG. 3. (Color online) Unit triangle of oxygen ions with a spread angle θ with respect to the c axis. $\theta \approx 90°$ for the MnO_5 cluster and $\theta = 56° - 72°$ for the YO_8 cluster.

(Mn $3d$-O_P $2p$). The apical hybridization for each bond is easily expressed with the Slater-Koster transfer integrals in the following:

$$V^2_{00,A} = V^2_{pd\sigma}, \quad V^2_{11,A} = V^2_{-1-1,A} = V^2_{pd\pi} \tag{5}$$

and all other $V_{mm',A}$ are zero, where the subscript A represents the hybridization with the apical oxygen.

The planar hybridization is rather intriguing because the symmetry of the electron cloud at three planar oxygen sites (threefold symmetry) cannot be directly converted to the d symmetry [twofold for yz/zx and fourfold for $(x^2-y^2)/xy$]. Thus, we first calculate the contribution of the planar oxygen triangle. Suppose that each oxygen ion in the triangle is located at a unit distance from the central ion with an angle θ from the c axis, as shown in Fig. 3. The Mn $3d$-O $2p$ hybridization strengths for the triangular oxygen ions are as follows:

$$V^2_{00,P} = \frac{3}{4}(1 - 3\cos^2\theta)^2 V^2_{pd\sigma} + \frac{9}{4}\sin^2 2\theta\, V^2_{pd\pi},$$

$$V^2_{\pm1\pm1,P} = \frac{9}{8}\sin^2 2\theta\, V^2_{pd\sigma} + \frac{3}{2}(\cos^2\theta + \cos^2 2\theta) V^2_{pd\pi},$$

$$V^2_{\pm2\pm2,P} = \frac{9}{8}\sin^4\theta\, V^2_{pd\sigma} + \frac{3}{2}\sin^2\theta(1 + \cos^2\theta) V^2_{pd\pi}, \tag{6}$$

$$V^2_{\pm2\mp1,P} = \frac{3\sin^2 2\theta\{9(3 - 4\cos 2\theta + \cos 4\theta)V^4_{pd\sigma} + 16(3 + \cos 4\theta)V^4_{pd\pi}\}}{32\{9(1 - \cos 4\theta)V^2_{pd\sigma} + 4(4 + \cos 2\theta + 3\cos 4\theta)V^2_{pd\pi}\}}, \tag{7}$$

where the subscript P represents the hybridization with the planar oxygen.

In MnO_5, θ is approximately $\pi/2$. Thus the off-diagonal terms $V_{\pm2\mp1}$, which do not vanish in general, become negligible, and each diagonal term becomes reduced to each orbital hybridization. The total hybridization strength, which corresponds to a sum of the apical and planar contributions, is given as follows:

$$V^2_{00} = V^2_{3z^2-r^2} = 2V^2_{pd\sigma} + \frac{3}{4}V^2_{pd\sigma}\kappa^7,$$

$$V^2_{\pm1\pm1} = V^2_{yz,zx} = 2V^2_{pd\pi} + \frac{3}{2}V^2_{pd\pi}\kappa^7,$$

$$V^2_{\pm2\pm2} = V^2_{x^2-y^2,xy} = \left(\frac{9}{8}V^2_{pd\sigma} + \frac{3}{2}V^2_{pd\pi}\right)\kappa^7. \tag{8}$$

Here κ^7 is introduced for the planar hybridization strengths according to the Harrison's a^{-7} rule. With an empirical relation $V_{pd\sigma} = -2V_{pd\pi}$, which is commonly adopted, the hybridization ratios of the d orbitals can be determined with the single contraction factor κ. In $YMnO_3$ with $\kappa = 0.9$, the hybridization strength of a_{1g} orbital, $V^2_{3z^2-r^2}$, is approximately 3.3 times larger than those of e_{1g} and e_{2g} orbitals, $V^2_{yz,zx}$ and $V^2_{x^2-y^2,xy}$, which are very close to each other. It is worthy to note that, besides the anisotropic crystal field (see Sec. II A), the strong hybridization strength of a_{1g} orbital is expected to lead to strong anisotropy in the electronic structure of the MnO_5 cluster. Now $V^2_{x^2-y^2}$ is largely reduced in comparison with that in the MnO_6 octahedron since MnO_5 has the longer planar bond length, the smaller number of planar oxygen ions, and the mismatch between the bond and orbital directions (see the Appendix).

2. *Hybridization strengths of* YO_8

A YO_8 cage has two apical oxygen ions (O_P) and two triangles of planar oxygen ions (O_T) in a quasi-D_{3d} symmetry (see Fig. 1). Starting from Eqs. (5)–(7), we calculated the total hybridization strengths of Y $4d$ orbitals, which are listed in Table I. The off-diagonal term ($V_{2-1} = V_{-21}$) is smaller than the diagonal terms and the hybridization strengths were found to be rather isotropic, indicating that

TABLE I. The relative hybridization strengths of Y $4d$ orbitals for $YMnO_3$ with $P6_3cm$ symmetry with respect to $V^2_{3z^2-r^2}$ of Y^2. Here, $V^2_{yz} = V^2_{zx}$, $V^2_{x^2-y^2} = V^2_{xy}$, and $V^2_{2-1} \equiv |\langle 2|-1\rangle|^2 = |\langle d_{xy}|\Psi_{zx}(O_8)\rangle|^2$. The empirical values are used for the Slater-Koster transfer integral ratios $V_{pd\sigma}/V_{pd\pi} = -2$ (Ref. 20).

	Y $4d$-O $2p$			
Site	$V^2_{3z^2-r^2}$	V^2_{zx}	V^2_{xy}	V^2_{2-1}
Y^1	1.183	1.196	1.223	0.211
Y^2	1	1.151	1.299	0.234

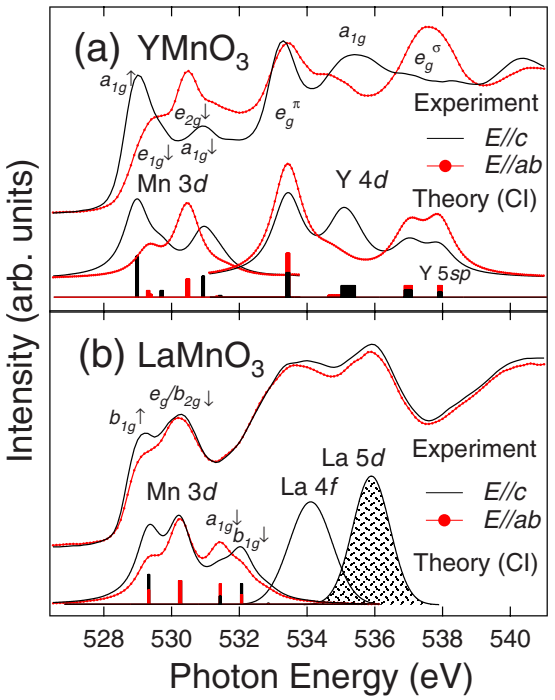

FIG. 4. (Color online) Polarization-dependent O K-edge XAS spectra of (a) hexagonal $YMnO_3$ and (b) orthorhombic $LaMnO_3$ (Ref. 11). The calculated eigenstates and spectral weights for (a) MnO_5 (D_{3h}) and YO_8 (D_{3d}) and (b) MnO_6 (D_{4h}) are presented with bars. Their broadened features show good agreement with the experimental spectra.

the overall electronic structure of Y 4d is dominated by the CF splittings.

III. X-RAY-ABSORPTION SPECTRA

From the calculated crystal fields and hybridization strengths in MnO_5 and YO_8 clusters, the polarization-dependent XAS spectra of $YMnO_3$ at O K and Mn $L_{2,3}$ edges are simulated in terms of the cluster model calculations with CIs including full atomic multiplets. The strict dipole selection rules enable us to identify the spectral features confidentially since the available XAS final states varies with the different polarizations. For comparison, the spectra of orthorhombic $LaMnO_3$ with MnO_6 (D_{4h}) in $Pbnm$ crystal structure,[21] which exhibits remarkably different spectral line shapes at O K and Mn $L_{2,3}$ edges in spite of the same ground-state electron number (d^4), are also examined using the similar physical parameter set except the site symmetry-dependent parameters such as the CF energies and the Mn 3d-O 2p hybridization strengths under the D_{4h} symmetry.

A. O K-edge absorption spectra

Figure 4(a) shows the polarization-dependent O K-edge XAS spectra of hexagonal $YMnO_3$ and the cluster model calculation results. The spectra display the O 2p states hybridized with Mn 3d/Mn 4sp and Y 4d/Y 5sp orbitals, and the calculation results successfully reproduce all the main features and their energy separations for both polarizations, $E\|c$ and $E\|ab$. The sp states provide rather broad spectral backgrounds. In the calculations, we took ratios of the CF splitting energies and hybridization strengths for different Mn 3d and Y 4d orbitals presented in Sec. II. The CF splitting energies and hybridization matrix elements are presented in Table II. Here the O 1s core-hole energy difference in the final state for the two oxygen sites (O_T and O_P) was considered to be $E(O_P)-E(O_T)=0.4$ eV, which was estimated from the O 1s photoemission spectrum (not shown here). The observed exchange energy, $E(3z^2-r^2,\downarrow)-E(3z^2-r^2,\uparrow)=1.9$ eV, is much smaller than the result of Hartree-Fock calculation[22] for Mn^{3+} ion (3–4 eV). The reduction in the exchange energy (i.e., F^2_{dd} and F^4_{dd}) might originate from the wave-function spreading due to rather strong hybridization with O 2p in this bipyramidal structure. The large hybridization strength of a_{1g} ($3z^2-r^2$) orbital increases the effective crystal-field splitting energy considerably. The Y 4d level split and the hybridization strengths in YO_8 cluster are remarkably larger than those in MnO_5. Y 4d e_g^π, a_{1g}, and e_g^σ orbital states contribute three main features around 533.5, 535, and 537 eV, respectively. The feature near 538 eV in $E\|ab$ spectra might be originated from the incorporation with Y 5sp-O 2p hybridization.

Figure 4(b) shows the O K-edge XAS spectra of the orthorhombic $LaMnO_3$ with MnO_6 (D_{4h}) and the model calculation results. The spectra are dominated by the Mn 3d ($h\nu$=528 eV–532 eV) and La 4f/5d states ($h\nu$

TABLE II. The crystal-field splitting energies and hybridization matrix elements of Mn/Y d-O 2p in hexagonal $YMnO_3$ deduced from the cluster model analysis and the LDA+U calculation. The crystal field and overall splitting energies of Y 4d a_{1g} state presents the average values for the Y^1 and Y^2 sites with an ~0.5 eV difference.

Method	Energy (eV)	Mn 3d			Y 4d		
		e_{1g}	e_{2g}	a_{1g}	e_g^π	a_{1g}	e_g^σ
Cluster model	Bare crystal field	0	0.5	1.1	0	~1.5	3.0
	Hybridization	2.1	2.1	3.8	6.5	6.0	6.5
	Overall split	0	0.7	1.5	0	~1.7	3.5
LDA+U	Hybridization	2.2	2.4	3.6	5.5	5.6	5.5
	Overall split	0	0.4	0.9	0	1.7	3.8

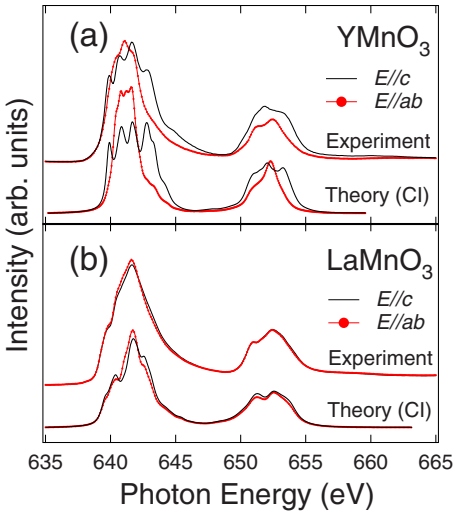

FIG. 5. (Color online) Polarization-dependent Mn $L_{2,3}$-edge XAS spectra of (a) hexagonal $YMnO_3$ and (b) orthorhombic $LaMnO_3$ (Ref. 11). The calculated spectra for (a) $MnO_5(D_{3h})$ and (b) $MnO_6(D_{4h})$ agree well with the experimental spectra.

=532 eV–538 eV). The Mn 3*d* region consists of two major features of $b_{1g}^{\uparrow}$ (x^2-y^2) and $e_g^{\downarrow}/b_{2g}^{\downarrow}$ (xy,yz,zx) at low and high energies, respectively. Here the *z* direction is defined as along the elongation direction of the MnO_6 octahedron.[23] The CF splitting energy, e_g-b_{1g}, is 1.2 eV and the hybridization matrix element, $V(x^2-y^2)=3.4$ eV, and the exchange energy, $E(x^2-y^2,\downarrow)-E(x^2-y^2,\uparrow)$, is 2.7 eV. The $a_{1g}^{\downarrow}/b_{1g}^{\downarrow}$ states appear as shoulders of the broad La $4f/5d$ features at $h\nu\sim534$ and ~536 eV, consistent with first-principles calculation results.[24–26]

B. Mn $L_{2,3}$-edge absorption spectra

The Mn $L_{2,3}$-edge XAS spectra display complicated but characteristic multiplet structure of the Mn $2p$-$3d$ Coulomb interactions at the final state. The spectra were theoretically simulated by using the cluster model calculations with the configuration interactions and the theoretical spectra well reproduce the overall line shapes. The calculations were performed for $d^n \oplus d^{n+1}\underline{p} \oplus d^{n+2}\underline{p}^2$ ($\underline{p}$: oxygen $2p$ hole) with full atomic multiplets. We adopted nearly the identical physical parameter set including the O $2p$ to Mn $3d$ charge-transfer energy Δ, Hubbard U, CF splitting energies,[27] and O $2p$-Mn $3d$ hybridization *V* as in the calculations for the O *K*-edge XAS discussed above. The quality of simulation is maintained only for less than 10% variations of the parameter values.

Figure 5 shows the polarization-dependent Mn $L_{2,3}$-edge XAS spectra and their theoretical simulations of (a) $YMnO_3$ and (b) $LaMnO_3$. The XAS spectrum shows large polarization dependence for $YMnO_3$ but relatively small variations for $LaMnO_3$ in the line shape as in the O *K*-edge XAS. In hexagonal $YMnO_3$, all the apical oxygen atoms locate along the crystal *c* axis and the polarization-dependent measurement fully takes into account the structural anisotropy while in orthorhombic $LaMnO_3$, the *z* direction elongation of the MnO_6 octahedron lies in the *ab* plane in a zigzag style and the structural anisotropy is partially reflected. However, even considering the partial reflection of the structural anisotropy in $LaMnO_3$, the polarization dependence of the XAS spectrum in $YMnO_3$ is so large that it cannot be simply attributed to the structural anisotropy. This result indicates that there should be an additional bonding anisotropy in the MnO_5 bipyramid, which enhances the orbital anisotropy in hexagonal $YMnO_3$ (see the Appendix).

IV. COMPARISON WITH RESULTS OF THE LDA+U CALCULATION

Now it is worthy to compare the CF splitting energies and the hybridization strengths of Mn $3d$ and Y $4d$ orbitals in $YMnO_3$, obtained in Sec. III, with the LDA+U results, whose details were presented elsewhere.[28] The Mn $3d$-O $2p$ and Y $4d$-O $2p$ hybridization strengths can be extracted from the LDA+U unoccupied O $2p$ partial density of states (PDOS) in the first-order approximation ($d^n \oplus d^{n+1}\underline{p}$); the configuration matrix yields a simple relation $V/\bar{\Delta}=a/(1-a^2)$, where *a* is the square root of the O $2p$ PDOS scaled by the Mn $3d$ (Y $4d$) PDOS and Δ is the O $2p$ to Mn $3d$ (Y $4d$) charge-transfer energy. Here Δ values for Mn $3d$ and Y $4d$ are adopted to be 4.0 and 8.0 eV, respectively.

The Mn $3d$/Y $4d$-O $2p$ hybridization matrix elements and the overall peak-to-peak splitting energies deduced from LDA+U are presented in Table II. These values are in good agreement with those determined in the cluster model analysis (Sec. III) except for minor differences in the Mn $3d$ splitting energies. The Mn $3d$ exchange energy, i.e., $E(3z^2-r^2,\downarrow)-E(3z^2-r^2,\uparrow)=2.3$ eV is slightly larger than the cluster model calculation result (1.9 eV). It is because the XAS final states reflect the one-electron additional conduction band, i.e., the $(N+1)$-electron system, which reduces the exchange energy (F_{dd}^2 and F_{dd}^4).

V. SUMMARY AND CONCLUSIONS

The experimental and theoretical studies on the O *K*- and Mn $L_{2,3}$-edge XAS of hexagonal $YMnO_3$ and orthorhombic $LaMnO_3$ revealed that the local site symmetry makes significant influences on the electronic structure of the manganite. We provided an algebraic formalism for the calculation of the CF energies and the hybridization strengths in MnO_5 (D_{3h}) and YO_8 (D_{4h}) clusters in $YMnO_3$, which are in good agreement with those extracted from the LDA+U calculation results. The cluster model calculations with the CF energies and hybridization strengths successfully reproduce the observed polarization-dependent XAS spectra. The general algebraic formalism in the unusual bipyramid MO_5 can be extended to studies on various hexagonal manganites $RMnO_3$ (Refs. 3, 5, and 7) and ferrites such as $LuFe_2O_4$,[29] which have taken so much attention since the discoveries of their interesting magnetic and ferroelectric behaviors.

ACKNOWLEDGMENTS

This work was supported by the KOSEF through the Acceleration Research Program (ARP No. R17-2008-033-

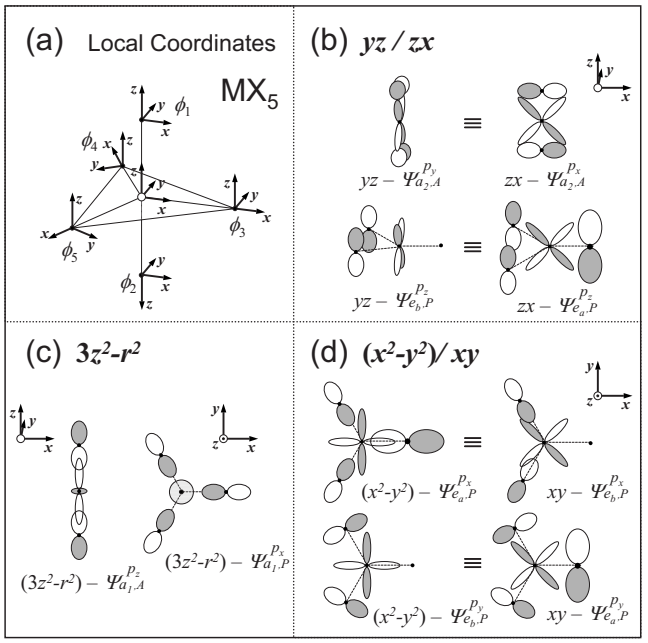

FIG. 6. (a) Convention for local coordinates for the five ligand orbitals and the central orbital in MX_5 bipyramid and ten orbital configurations of nonvanishing M d-X p overlaps for the (b) d_{yz}/d_{zx}, (c) $d_{3z^2-r^2}$, and (d) $d_{x^2-y^2}/d_{xy}$ orbitals. Equality in (b) and (d) indicates that the two have essentially the same orbital overlap.

01000-0) at SNU and eSSC at POSTECH, the KOSEF under Grant No. R01-2007-000-11188-0, POSTECH research fund, and BK21 program.

APPENDIX: HYBRIDIZATION IN MX_5 BIPYRAMID

Here we derive Eq. (8) in a formal way. For calculating the hybridization strengths, it is convenient to compare bipyramid (MX_5; D_{3h} symmetry) with octahedron (MX_6; O_h symmetry). First, the number of planar ligands of the bipyramid is different from the octahedron. It is reduced from 4 to 3, so that the total *planar* hybridization strength should be 3/4 of octahedron case. Second, there is a contraction factor $\kappa = d(M-X_A)/d(M-X_P)$, where the subscripts A and P represent the apical and planar ligands, respectively.

Each ligand contributes three p orbitals, resulting in 15 ligand p orbital states ϕ_n^j ($j=p_x,p_y,p_z$), where n (=1,2,3,4,5) stands for five ligand sites and the x coordinate of each ligand X_n can be chosen for convenience along the M-X_n bond direction as shown in Fig. 6(a). Utilizing the ligand group theory, we can build symmetrized wave functions Ψ's for the bipyramidal D_{3h} symmetry from the orbital states ϕ_n^j's.[13] The six states related to the apical ligands $X_{1,2}$ and the nine states to the planar ligands $X_{3,4,5}$ are separated due to the symmetry as in Eqs. (A1) and (A3), respectively.

The apical wave functions have symmetric and antisymmetric forms

$$\Psi^j_{a_1,A} = 1/\sqrt{2}(\phi_1^j + \phi_2^j),$$

$$\Psi^j_{a_2,A} = 1/\sqrt{2}(\phi_1^j - \phi_2^j), \quad j = p_x,p_y,p_z. \tag{A1}$$

Only three out of the six wave functions have nonvanishing overlap integrals with M d orbitals.

$$|\langle 3z^2 - r^2 | \Psi^{p_z}_{a_1,A}\rangle|^2 = 2,$$

$$|\langle zx | \Psi^{p_x}_{a_2,A}\rangle|^2 = |\langle yz | \Psi^{p_y}_{a_2,A}\rangle|^2 = 2. \tag{A2}$$

Note that all three integrals have a value of 2, which accounts for the number of the apical ligands, the same as in the case of the MX_6 octahedron.

The planar hybridizations, however, are rather different from those in the octahedron. The planar ligand ions have three different symmetries as follows:

$$\Psi^j_{a_1,P} = 1/\sqrt{3}(\phi_3^j + \phi_4^j + \phi_5^j),$$

$$\Psi^j_{e_a,P} = 1/\sqrt{6}(2\phi_3^j - \phi_4^j - \phi_5^j),$$

$$\Psi^j_{e_b,P} = 1/\sqrt{2}(\phi_4^j - \phi_5^j), \quad j = p_x,p_y,p_z. \tag{A3}$$

One intriguing point is that the planar ligand p orbitals with the threefold symmetry are not directly converted to the d-orbital symmetry [twofold for yz/zx and fourfold for $(x^2-y^2)/xy$]. Thus we formally decompose the p states into components with fourfold and twofold symmetries,

$$\Psi^j_{a_1,P} = \frac{1}{\sqrt{3}}\sum_{\eta(n)} \phi_n^j,$$

$$\Psi^j_{e_a,P} = \frac{1}{\sqrt{6}}\sum_{\eta(n)} (e^{2i\eta} + e^{i\eta})\phi_n^j,$$

$$\Psi^j_{e_b,P} = \frac{i}{\sqrt{6}}\sum_{\eta(n)} (e^{2i\eta} - e^{i\eta})\phi_n^j, \tag{A4}$$

where η stands for the rotation angles 0, $\frac{2}{3}\pi$, and $\frac{4}{3}\pi$ of the planar ligands $n=3$, 4, and 5, respectively.

The projected phase states of d orbitals correspond to $|e^{2i\eta}\rangle$ for $(x^2-y^2)/xy$, $|e^{i\eta}\rangle$ for yz/zx, and $|e^{i0}\rangle$ for $3z^2-r^2$. Here seven out of the nine wave functions have the nonvanishing overlap integrals,

$$|\langle 3z^2 - r^2 | \Psi^{p_x}_{a_1,P}\rangle|^2 = 3,$$

$$|\langle zx | \Psi^{p_z}_{e_a,P}\rangle|^2 = |\langle yz | \Psi^{p_z}_{e_b,P}\rangle|^2 = 3,$$

$$|\langle x^2 - y^2 | \Psi^{p_x}_{e_a,P}\rangle|^2 = |\langle xy | \Psi^{p_x}_{e_b,P}\rangle|^2 = 3,$$

$$|\langle xy | \Psi^{p_y}_{e_a,P}\rangle|^2 = |\langle x^2 - y^2 | \Psi^{p_y}_{e_b,P}\rangle|^2 = 3. \tag{A5}$$

This value again corresponds to the number of planar ligands. It means that the planar hybridization strength in the bipyramid is smaller by a factor of 3/4 than that in the octahedron with four planar ligands. For insight, orbital configurations for the ten nonvanishing integrals are schematically

cartooned in Figs. 6(b)–6(d). The equalities in the figure indicate essentially equal orbital overlaps for the $pd\pi$ and $pd\sigma$ bonds, represented as equalities between the overlap integrals in Eqs. (A2) and (A5). The overlap integrals of $\Psi^{p_{x,y}}_{a_{2'},A}$ in Eq. (A2) have the same form as can be seen in Fig. 6(b) and its equality is trivial. The equalities between the overlap integrals of $\Psi^{j}_{e_{a'},P}$ and $\Psi^{j}_{e_{b'},P}$ for the respective j can be verified by noting that the coefficient of either $e^{2i\eta}$ term (for x^2-y^2/xy) or $e^{i\eta}$ term (for yz/zx) in $\Psi^{j}_{e_{a'},P}$ has the same modulus $(1/\sqrt{6})$ with that in $\Psi^{j}_{e_{b'},P}$ in Eq. (A4).

The total hybridization strength of each d orbital over all ligand p states, which corresponds to the sum of the planar and apical contributions, can be expressed in terms of the Slater-Koster transfer integrals $V_{pd\sigma}$ and $V_{pd\pi}$. First we take advantage of knowledge for the M d-X p hybridization strengths in the MX_6 octahedron with two apical and four planar ligands as

$$V^2_{3z^2-r^2} = 2V^2_{pd\sigma,A} + 4\cdot\frac{1}{4}V^2_{pd\sigma,P},$$

$$V^2_{yz/zx} = 2V^2_{pd\pi,A} + 4\cdot\frac{1}{2}V^2_{pd\pi,P},$$

$$V^2_{x^2-y^2} = 4\cdot\frac{3}{4}V^2_{pd\sigma,P} = 3V^2_{pd\sigma,P},$$

$$V^2_{xy} = 4V^2_{pd\pi,P}. \tag{A6}$$

Now we apply the different number of planar ligands in the MX_5 bipyramid for the hybridization strengths,

$$V^2_{3z^2-r^2} = 2V^2_{pd\sigma,A} + 3\cdot\frac{1}{4}V^2_{pd\sigma,P},$$

$$V^2_{yz/zx} = 2V^2_{pd\pi,A} + 3\cdot\frac{1}{2}V^2_{pd\pi,P},$$

$$V^2_{x^2-y^2/xy} = \frac{3}{4}\cdot\frac{1}{2}(3V^2_{pd\sigma,P} + 4V^2_{pd\pi,P}). \tag{A7}$$

Here the total hybridization strengths of x^2-y^2 and xy, which are the same, should be obtained by applying the factor of 3/4 on the average of the corresponding x^2-y^2 and xy hybridization strengths, which are different from each other in the octahedron. Finally, the hybridization strengths of the d orbitals can be determined after consideration of the contraction factor κ,

$$V^2_{3z^2-r^2} = 2V^2_{pd\sigma} + \frac{3}{4}V^2_{pd\sigma}\kappa^7,$$

$$V^2_{yz/zx} = 2V^2_{pd\pi} + \frac{3}{2}V^2_{pd\pi}\kappa^7,$$

$$V^2_{x^2-y^2/xy} = \left(\frac{9}{8}V^2_{pd\sigma} + \frac{3}{2}V^2_{pd\pi}\right)\kappa^7. \tag{A8}$$

These are exactly the same as in Eq. (8).

*Present address: Department of Materials Science and Engineering, Seoul National University, Seoul 151-744, Korea.
†Author to whom correspondence should be addressed. jhp@postech.ac.kr

[1] G. A. Smolenskii and I. E. Chupis, Usp. Fiziol. Nauk **137**, 415 (1982).
[2] T. Katsufuji, S. Mori, M. Masaki, Y. Moritomo, N. Yamamoto, and H. Takagi, Phys. Rev. B **64**, 104419 (2001).
[3] M. Fiebig, Th. Lottermoser, D. Fröhlich, A. V. Goltsev, and R. V. Pisarev, Nature (London) **419**, 818 (2002).
[4] Th. Lottermoser, Th. Lonkai, U. Amann, D. Hohlwein, J. Ihringer, and M. Fiebig, Nature (London) **430**, 541 (2004).
[5] A. B. Souchkov, J. R. Simpson, M. Quijada, H. Ishibashi, N. Hur, J. S. Ahn, S.-W. Cheong, A. J. Millis, and H. D. Drew, Phys. Rev. Lett. **91**, 027203 (2003).
[6] C. R. Serrao, S. B. Krupanidhi, J. Bhattacharjee, U. V. Waghmare, A. K. Kundu, and C. N. R. Rao, J. Appl. Phys. **100**, 076104 (2006).
[7] S. Lee, A. Pirogov, M. Kang, K.-H. Jang, M. Yonemura, T. Kamiyama, S.-W. Cheong, F. Gozzo, N. Shin, H. Kimura, Y. Noda, and J.-G. Park, Nature (London) **451**, 805 (2008).
[8] B. B. van Aken, T. T. M. Palstra, A. Filippetti, and N. A. Spaldin, Nature Mater. **3**, 164 (2004).
[9] A. Muñoz, J. A. Alonso, M. J. Martínez-Lope, M. T. Casáis, J. L. Martínez, and M. T. Fernández-Díaz, Phys. Rev. B **62**, 9498 (2000).
[10] A. Filippetti and N. A. Hill, Phys. Rev. B **65**, 195120 (2002).
[11] D.-Y. Cho, J.-Y. Kim, B.-G. Park, K.-J. Rho, J.-H. Park, H.-J. Noh, B.-J. Kim, S.-J. Oh, H.-M. Park, J.-S. Ahn, H. Ishibashi, S.-W. Cheong, J.-H. Lee, P. Murugavel, T. W. Noh, A. Tanaka, and T. Jo, Phys. Rev. Lett. **98**, 217601 (2007).
[12] S. Lee, A. Pirogov, J. H. Han, J.-G. Park, A. Hoshikawa, and T. Kamiyama, Phys. Rev. B **71**, 180413(R) (2005).
[13] B. E. Douglas and C. A. Hollingsworth, *Symmetry in Bonding and Spectra* (Academic, New York, 1985).
[14] T. Iizuka-Sakano, E. Hanamura, and Y. Tanabe, J. Phys.: Condens. Matter **13**, 3031 (2001).
[15] T. Katsufuji, M. Masaki, A. Machida, M. Moritomo, K. Kato, E. Nishibori, M. Takata, M. Sakata, K. Ohoyama, K. Kitazawa, and H. Takagi, Phys. Rev. B **66**, 134434 (2002).
[16] S. Sugano, Y. Tanabe, and H. Kamimura, *Multiplets of Transition-Metal Ions in Crystals* (Academic, New York, 1970).
[17] J. A. Gaunt, Philos. Trans. R. Soc. London, Ser. A **228**, 151 (1929).
[18] M. Nicastro and C. H. Patterson, Phys. Rev. B **65**, 205111 (2002).

[19] This ratio turns out to be consistent with the O *K*- and Mn $L_{2,3}$-edge XAS spectra (Ref. 11) and the second-harmonic experiment results [see, e.g., A. V. Kimel, R. V. Pisarev, F. Bentivegna, and T. Rasing, Phys. Rev. B **64**, 201103(R) (2001)].

[20] W. A. Harrison, *Electronic Structure and the Properties of Solids* (Freeman, San Fransisco, 1980).

[21] In this setting, electronic structures projected on the sample *c*-axis direction can be distinguished from those projected on the sample *ab* plane by the polarization-dependent spectroscopies [see, e.g., J. Rodríguez-Carvajal, M. Hennion, F. Moussa, A. H. Moudden, L. Pinsard, and A. Revcolevschi, Phys. Rev. B **57**, R3189 (1998)].

[22] R. D. Cowan, *The Theory of Atomic Structure and Spectra* (University of California Press, Berkeley, 1981).

[23] The Mn-O bond lengths in $LaMnO_3$ are 1.91, 1.97, and 2.17 Å [C. Ritter, M. R. Ibarra, J. M. De Teresa, P. A. Algarabel, C. Marquina, J. Blasco, J. García, S. Oseroff, and S. W. Cheong, Phys. Rev. B **56**, 8902 (1997)]. Two shorter bonds can be approximated to be identical, so that the octahedron would have the D_{4h} symmetry.

[24] P. Ravindran, A. Kjekshus, H. Fjellvåg, A. Delin, and O. Eriksson, Phys. Rev. B **65**, 064445 (2002).

[25] S. Satpathy, Z. S. Popović, and F. R. Vukajlović, Phys. Rev. Lett. **76**, 960 (1996).

[26] D. Muñoz, N. M. Harrison, and F. Illas, Phys. Rev. B **69**, 085115 (2004).

[27] U and Δ's were 4.0–4.5 eV and the Mn 2*p*-3*d* Coulomb energies (U_{pd}) were 5.0–5.5 eV for both manganites. The Slater integrals were taken as (50–80)% of the atomic Hartree-Fock values to account for the spread of the 3*d* wave functions in the crystal. For the Mn $L_{2,3}$-edge XAS simulation, the CF splitting energies (the Slater integrals) were reduced (enhanced) by $\lesssim$25% ($\lesssim$10%) from the values for the O *K* edge's (Table II) to account for the core-hole effects.

[28] W. S. Choi, D. G. Kim, Sung Seok A. Seo, S. J. Moon, D. Lee, J. H. Lee, H. S. Lee, D. Y. Cho, Y. S. Lee, P. Murugavel, J. Yu, and T. W. Noh, Phys. Rev. B **77**, 045137 (2008).

[29] W. Wu, V. Kiryukhin, H. J. Noh, K. T. Ko, J. H. Park, W. Ratcliff, P. A. Sharma, N. Harrison, Y. J. Choi, Y. Horibe, S. Lee, S. Park, H. T. Yi, C. L. Zhang, and S. W. Cheong, Phys. Rev. Lett. **101**, 137203 (2008).